ELSEVIER

Fuel 79 (2000) 1611–1619

FUEL

www.elsevier.com/locate/fuel

Modelling of the combustion process and NO_x emission in a utility boiler

M. Xu[a,*], J.L.T. Azevedo[b], M.G. Carvalho[b]

[a]National Laboratory of Coal Combustion, Huazhong University of Science and Technology, Wuhan 430074, People's Republic of China
[b]Instituto Superior Técnico, Av. Rovisco Pais, 1096 Lisbon, Portugal

Accepted 19 January 2000

Abstract

This paper presents numerical simulation of the flow and combustion process in the furnace of a pulverized coal fired utility boiler of 350 MWe with 24 swirl burners installed at the furnace front wall. Five different cases with 100, 95, 85, 70 and 50% boiler full load are simulated. The comparison between the simulation and the plant data is stressed in this study. The heat flux to furnace walls between the measured values and the calculation results is compared. It is found that increasing the load leads to consistent variations in the properties presented and the exception is observed for the full load case where the predicted exit gas temperature is lower than the 95% one and the total heat to the boiler walls is smaller. This might be due to the fact of considering a linear scaling of the input parameters between the 70% and 100% load. The increase of the air flow rate led as expected to a reduction of the furnace outlet temperature and to a small decrease in NO_x emissions. It shows that the NO_x model used shows a higher sensitivity to temperature than to oxygen level in the furnace. The model used considered the De Soete mechanism for the nitrogen from volatiles and the contribution of char was considered in a similar way. The agreement for all cases except the one of 50% boiler load between the calculation results with the plant data validates the models and algorithm employed in the computation. The furnace performance under different boiler loads is predicted and compared in order to meet the requirements of NO_x abatement and avoiding some negative side effects on the furnace.

Keywords: Modelling; NO_x emission; Utility boiler

1. Introduction

The efficient use of pulverized coal is crucial to the utility industry. To achieve a higher combustion efficiency, the major affecting factors such as the particle size distribution, gas and particle temperatures, local heat release, local oxygen concentration, kinetic parameters for coal devolatilization and char oxidation, and coal properties should be understood thoroughly.

In the past two decades, the use of CFD codes for modelling utility boilers is becoming a useful tool to predict the performance of boilers among the scientific and industrial communities [1–8]. It helps engineers to optimize the operating conditions, reduce pollutant emissions, investigate malfunctions in the equipment, evaluate different corrective measures and also improve the design of new boilers. Submodels for simulating the in-furnace processes such as mixing, radiative heat transfer, and chemical kinetics have been developed. The development of the models depends on the availability of accurate and approximate experimental data for comparison. However, because of the expensive price of measurements of the combustion and heat transfer characteristics and the limitation by the geometry, time, and number of instruments and skills required, assessment of these models is still limited to laboratory-scale [9,10]. Only a few detailed works reported in the literature are concerned with power plants typically below 80 MWe [1,11–13]. This paper addresses the comparison between the predictions and measurements acquired in a pulverized coal-fired boiler of 350 MWe of the Spanish Empresa National de Electricidad, S.A. (ENDESA) with 24 swirl burner installed at the furnace front wall.

The improvement of boiler operation and the development of tools to assess these are continuously pursued. Primary measurements for NO_x reduction have been successfully implemented in power plants allowing to meet the stringent NO_x emission limits. However, in some cases, there is still the need to improve burner or boiler design with the objective of producing NO_x abatement avoiding some negative side effects such as the increase of unburned carbon in the fly ash and modifications in the fouling and slagging in the furnace and superheater surfaces. This paper also concentrates on the predicting of furnace performance for different boiler operating conditions.

* Corresponding author. Tel.: + 86-27-8754-2417; fax: + 86-27-8754-5526.
E-mail address: mhxu@mail.hust.edu.cn (M. Xu).

0016-2361/00/$ - see front matter
PII: S0016-2361(00)00019-3

Nomenclature

A_E	External char surface area ($m^2\ kg^{-1}$)
BO	Char burnout
$D_{NO,gas}$	Binary diffusion coefficient of NO in combustion product gases ($m^{-2}\ s^{-1}$)
d_p	Particle diameter (m)
f_N	Mass fraction of nitrogen in coal (dry)
k, k_1, k_2	Kinetic reaction rate (kg $kmol^{-1}$)
m_c	Mass of coal (kg)
m_{char}	Mass of char (kg)
M_i	Molar weight of species i (kg $kmol^{-1}$)
P	Total pressure (Pa)
R	Universal gas constant (J $kmol\ K^{-1}$)
S_{char}	Rate of char oxidation ($kg\ m^{-3}\ s^{-1}$)
S_{devol}	Rate of coal devolatilization ($kg\ m^{-3}\ s^{-1}$)
$S_{Dif,NO}$	Proportional factor for diffusion of NO from char ($kg\ m^{-3}\ s^{-1}$)
Sh	Sherwood number
$S_{i,NO}$	Source of NO ($kg\ m^{-3}\ s^{-1}$)
SR	Stoichiometric ratio
$S_{Thermal,NO}$	Source of thermal-NO ($kg\ m^{-3}\ s^{-1}$)
T	Temperature (K)
VOL	Volume (m^3)
X_i	Molar fraction of species i
X_{NOsup}	Molar fraction of NO at char surface
α	Mass fraction of HCN released by volatile
α_1, α_2	Mass stoichiometric factor (s^{-1})

The boiler geometry and operating conditions is described in Section 2, and is followed by the description of the mathematical model in Section 3. Then the results are presented and discussed in Section 4. Finally, the paper ends with a summary of the main conclusions in Section 5.

2. Boiler geometry and cases description

The data of boiler geometry were taken in one of the boilers of ENDESA, as shown in Fig. 1. The front wall pulverized coal fired boiler is 48.7 m high, 17.13 m wide, 10.67 m deep and with an installed capacity of 350 MWe. Twenty four burners are arranged in an array of four burners disposed in six different levels. The boiler operating conditions considered in this study include full load (100%), 95, 85, 70 and 50% boiler full load corresponding to cases with all burners in service (100, 95 and 85%), 1–4 and 6 rows (from the bottom) of burners in service, 1 and 3–5 rows of burners in service, respectively. All the boiler operating conditions are listed in Table 1. Among them, cases 100, 70 and 50% are the raw cases from the power plant and cases 95 and 85% are interpolated from cases 100 and 70%.

Besides the above simulation for different boiler loads, corresponding cases of higher excess oxygen levels (more secondary air flow rate) were also calculated to predict the performance of the boiler and validate NO_x models applied in this study.

3. Mathematical models

The mathematical model is based on an Eulerian description for the continuum phase and a stochastic Lagrangean description for the coal particles while the following assumptions are made. (1) The mass sources are provided by the three-dimensional flow at levels corresponding to burner positions. (2) Burner mixing is characterized by the turbulence intensity of the burner. The production of turbulence and its dissipation are modelled with k–ε model. (3) The polydisperse distribution of coal is segmented into discrete particle groups, assuming Rosin–Rammler distribution. (4) A simple chemically reacting system (SCRS) is adopted where the reaction rates are very fast compared with the mixing rates. (5) Char oxidizes to CO at the particle surface; CO oxidizes to CO_2 in the bulk gas.

The well-known k–ε eddy viscosity/diffusivity model is used to quantify turbulent mixing in the furnace. The representative coal particles are tracked in the combustion chamber using simulated instantaneous gas velocities. The energy balance to the coal particles is used to calculate the particle temperature with time and to describe coal evolution. Char combustion is modelled using a parallel process of surface kinetics and oxygen diffusion. The balance of radiative heat transfer is calculated using the discrete transfer method [14] which is based on the direct solution of the radiation intensity transport equation. The radiative properties of gas are computed using the wide band model. Detailed description of the models is presented in Refs. [15–18].

The velocity, the temperature and the mixture fraction are prescribed at the inlet, whereas the kinetic energy of the turbulence and its dissipation rate are estimated (see, for example, Carvalho, et al. [19]). At the walls, the laws of the wall [20] are employed. Although this approach may be questionable in respect of heat transfer in complex recirculating flows [21], it does not present a serious problem for the present application. In fact, heat transfer to the walls in utility boilers is mainly due to radiation and the convective heat transfer has only a minor contribution. The temperature and emissivity of the walls are specified. At the exit, a zero gradient normal to the boundary is assumed for the dependent variables. The vertical velocity is then corrected to ensure mass conservation.

A post processor is employed for NO_x simulation based on an extension of De Soete's mechanism ([22]) schematically illustrated in Fig. 2. The model is developed on the basis of the solution of balance equations involving NO and its precursors (HCN and NH_3) assuming $\alpha = 0.9$. The mechanism for volatiles is extended to include thermal NO_x, reburning and NO_x formation from coal char. The

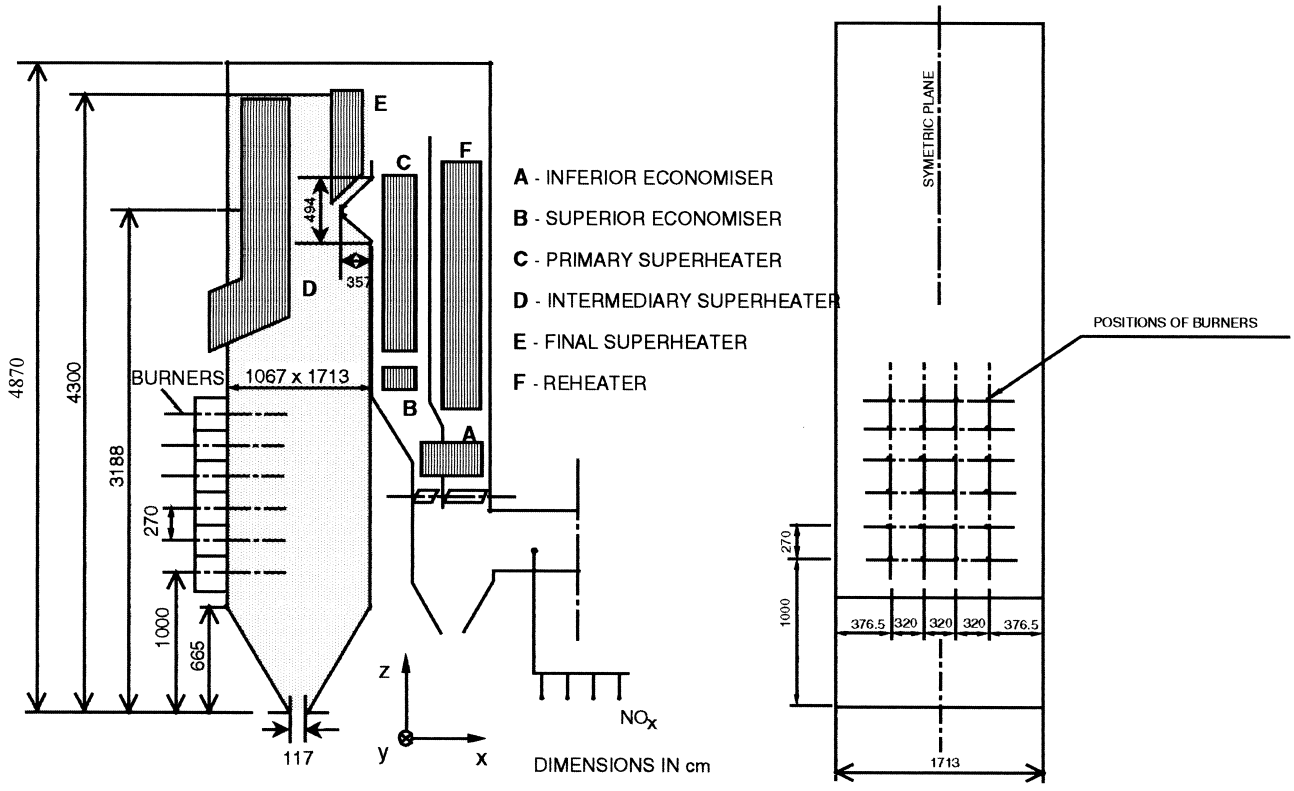

Fig. 1. Sketch of the utility boiler.

nitrogen in coal is assumed to be uniformly divided by the char and volatile matter. For the reburning reaction, the kinetic rate presented by Chen [23] is used together with the eddy break-up model. The kinetic rate derived represents the global reaction rate between light hydrocarbons and NO_x.

The volatile composition can be determined from the parallel volatilization model [24,25] described below which indicates the fraction of CH_4 to account for 10% of the volatile mass release. The parallel volatilization model represents the overall devolatilization process by two mutually competing first order reactions. The rate of weight loss of the coal (d.a.f.) is given by

$$\frac{dm_c}{dt} = -(k_1 + k_2)m_c \quad (1)$$

The rate of devolatilization at any time is

$$\frac{dV}{dt} = (\alpha_1 k_1 + \alpha_2 k_2)m_c \quad (2)$$

and the extent of devolatilization at time t is obtained as

$$V(t) = m_c(0)\int_0^t (\alpha_1 k_1 + \alpha_2 k_2)\exp\left[-\int_0^{t'}(k_1 + k_2)\,dt'\right]dt \quad (3)$$

In the above set of equations, α_1 and α_2 are mass stoichiometric factors denoting the extents of devolatilization via reactions 1 and 2, respectively. The rate constants k_1 and k_2 have Arrhenius form, and are such that reaction-1 has a lower activation energy than reaction-2, with the effect

Table 1
Cases description (*Note*: VM—volatile matter; PA—primary air; SA—secondary air)

Case no.	1	2	3	4	5	6	7	8	9	10
Boiler load (%)	100	95	85	70	50	100	95	85	70	50
Rows of burner in service	1–6	1–6	1–6	1–4,6	1,3–5	1–6	1–6	1–6	1–4,6	1,3–5
N mass fraction in coal (%)	0.54	0.56	0.625	0.66	0.67	0.54	0.56	0.625	0.66	0.67
VM in coal (%)	25.76	25.795	25.865	25.97	24.22	25.76	25.795	25.865	25.97	24.22
Total coal flow rate (t/h)	205	198.6	185.6	166.2	119.2	205	198.6	185.6	166.2	119.2
Total PA flow rate (t/h)	352.8	335.8	301.7	250.7	200.0	352.8	335.8	301.7	250.7	200.0
Total SA flow rate (t/h)	930.4	921.5	903.7	877.0	734.7	1022.7	1008.6	980.4	938.2	826.9

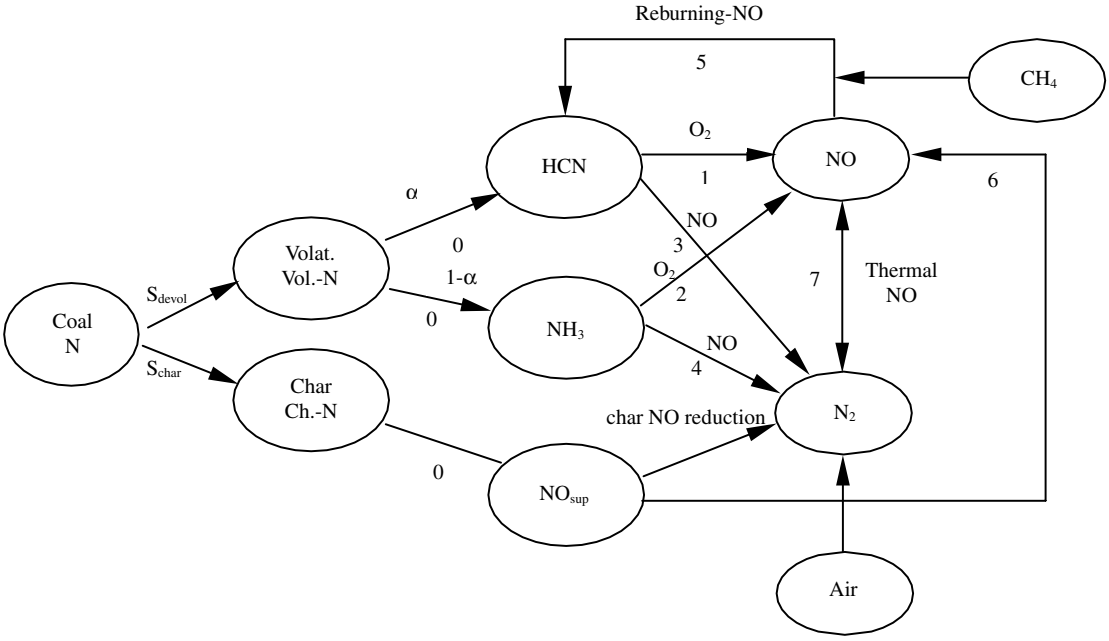

Fig. 2. Schematic diagram of global NO formation mechanism.

that the second reaction becomes operational only at higher temperatures to effect volatile yields in excess of α_1.

Most of the volatile matter is released as tar which will decompose later into lighter hydrocarbons and their radicals but no attempt is made here to simulate these. The reburning reaction rate taken from Chen [23] is considered between NO and methane from volatile and the natural gas. The oxidation rate of methane is higher than that of other volatile species and therefore its concentration can be lower than the fraction of volatile matter considered.

Methane is competitively consumed by combustion and by the reburning reaction. The reaction rate of the latter is slower than the oxidation and therefore the calculations are performed considering that for the reburning reaction methane would be left if complete oxidation occurs. The reburning reaction is considered in the fuel rich zones together with Eqs. (5b) and (7b). These equations are a modification of the reaction rates from De Soete's model while Eqs. (5a) and (7a) are employed for fuel lean conditions with the constant in Eq. (5a) increased by 3.5 compared with the original value proposed by Lockwood and Romo-Millares [26]. The calculation of NO formation from char is considered by the balance of concentration at the particle surface. All char nitrogen is assumed to produce NO at the particle surface proportionally to the char consumption rate (Eq. (10b)). Simultaneous NO reduction is calculated based on its concentration close to the particle surface (Eq. (10c)). The mass source of NO can be obtained from the difference of the two rates and the calculation of NO concentration at the char surface (Eq. (10a)) is obtained equating the source of diffusion flux from the particle to the surroundings (Eq. (10)). It should be noted that NO concentration at char surface can be larger than or smaller than the remote value which is calculated from the mass balance. Mean particle diameters are used in each control volume for the calculation of $S_{\mathrm{Dif,NO}}$

$$S_{0,\mathrm{HCN}} = 2\alpha f_{\mathrm{N}} S_{\mathrm{devol}} (M_{\mathrm{HCN}}/M_{\mathrm{N_2}}) \tag{4a}$$

$$S_{0,\mathrm{NH_3}} = 2(1-\alpha) f_{\mathrm{N}} S_{\mathrm{devol}} (M_{\mathrm{NH_3}}/M_{\mathrm{N_2}}) \tag{4b}$$

$$S_{1,\mathrm{NO}} = \rho \times 3.5 \times 10^{10} X_{\mathrm{HCN}} X_{\mathrm{O_2}}^{\mathrm{b}} \exp\left(-\frac{2.805 \times 10^8}{\mathrm{R}T}\right) \frac{M_{\mathrm{NO}}}{M_{\mathrm{gas}}} \tag{5a}$$

$$S_{1,\mathrm{NO}} = \rho \times 1.5 \times 10^{10} X_{\mathrm{HCN}} X_{\mathrm{O_2}}^{\mathrm{b}} \exp\left(-\frac{2.646 \times 10^8}{\mathrm{R}T}\right) \frac{M_{\mathrm{NO}}}{M_{\mathrm{gas}}} \tag{5b}$$

$$S_{2,\mathrm{NO}} = \rho \times 4.0 \times 10^{6} X_{\mathrm{NH_3}} X_{\mathrm{O_2}}^{\mathrm{b}} \exp\left(-\frac{1.340 \times 10^8}{\mathrm{R}T}\right) \frac{M_{\mathrm{NO}}}{M_{\mathrm{gas}}} \tag{6}$$

$$S_{3,\mathrm{NO}} = \rho \times 3.0 \times 10^{12} X_{\mathrm{HCN}} X_{\mathrm{NO}} \exp\left(-\frac{2.512 \times 10^8}{\mathrm{R}T}\right) \frac{M_{\mathrm{NO}}}{M_{\mathrm{gas}}} \tag{7a}$$

$$S_{3,\mathrm{NO}} = \rho \times 1.1 \times 10^{12} X_{\mathrm{HCN}} X_{\mathrm{NO}} \exp\left(-\frac{2.470 \times 10^8}{\mathrm{R}T}\right) \frac{M_{\mathrm{NO}}}{M_{\mathrm{gas}}} \tag{7b}$$

Table 2
Coal particle trajectory data

Number of particle start locations	4
Number of track paths per start locations	10
Maximum number of steps in each trajectory	500

$$S_{4,\mathrm{NO}} = \rho \times 1.8 \times 10^8 X_{\mathrm{NH_3}} X_{\mathrm{NO}} \exp\left(-\frac{1.131 \times 10^8}{\mathrm{R}T}\right)\frac{M_{\mathrm{NO}}}{M_{\mathrm{gas}}} \tag{8}$$

$$S_{5,\mathrm{NO}} = \rho \times 2.76 \times 10^6 X_{\mathrm{HC}} X_{\mathrm{NO}} \exp\left(-\frac{0.7872 \times 10^8}{\mathrm{R}T}\right)\frac{M_{\mathrm{NO}}}{M_{\mathrm{gas}}} \tag{9}$$

$$X_{\mathrm{HC}} = X_{\mathrm{CH_4}} - X_{\mathrm{O_2}}/\mathrm{SR}_{\mathrm{CH_4}} \tag{9a}$$

$$S_{6,\mathrm{NO}} = S_{\mathrm{Dif,NO}}(X_{\mathrm{NO}} - X_{\mathrm{NO_{sup}}}) = S_{0P,\mathrm{NO}} - S_{0R,\mathrm{NO}} X_{\mathrm{NO_{sup}}} \tag{10}$$

$$X_{\mathrm{NO_{sup}}} = \frac{S_{0P,\mathrm{NO}} + S_{\mathrm{Dif,NO}} X_{\mathrm{NO}}}{S_{0R,\mathrm{NO}} + S_{\mathrm{Dif,NO}}} \tag{10a}$$

$$S_{0P,\mathrm{NO}} = 2 f_{\mathrm{N}} S_{\mathrm{char}} (M_{\mathrm{NO}}/M_{\mathrm{N_2}}) \tag{10b}$$

$$S_{0R,\mathrm{NO}} = 4.24 \times 10^4 A_{\mathrm{E}} \frac{m_{\mathrm{char}}}{\mathrm{VOL}} P X_{\mathrm{NO_{sup}}} \times \exp\left(-\frac{1.465 \times 10^8}{\mathrm{R}T}\right) M_{\mathrm{NO}} \tag{10c}$$

$$S_{\mathrm{Dif,NO}} = A_{\mathrm{E}} m_{\mathrm{char}} \frac{Sh \times M_{\mathrm{NO}} D_{\mathrm{NO,gas}}}{\mathrm{R}T d_{\mathrm{p}}} \tag{10d}$$

$$S_{\mathrm{Thermal,NO}} = \rho \frac{2.0 X_{\mathrm{O}} (k_3 k_4 X_{\mathrm{O_2}} X_{\mathrm{N_2}} - k_{-3} k_{-4} X_{\mathrm{NO}}^2)}{k_4 X_{\mathrm{O_2}} + k_{-3} X_{\mathrm{NO}}} \frac{M_{\mathrm{NO}}}{M_{\mathrm{gas}}} \tag{11}$$

All the Eulerian partial differential equations governing conservation of mass, momentum and energy can be written in the following general form:

$$\frac{\partial(\rho u_j \phi)}{\partial x_j} = \frac{\partial}{\partial x_j}(\Gamma_\phi \frac{\partial \phi}{\partial x_j}) + S_\phi \tag{12}$$

where ϕ stands for the three momentum components, the turbulent kinetic energy k and its dissipation ε, the enthalpy, and the mass fraction of gas species (mixture fraction). Γ_ϕ is the diffusion coefficient of the transported variable ϕ. For the particular case of the mass conservation equation, variable ϕ is set to unity and the right-hand side of the equation is zero.

Table 3
Coal particle size distribution

d (μm)	200	130	90	70	50
Mass fraction (%)	0.5	3.0	5.0	10.5	81.0

Table 4
Coal combustion parameters

(a) *Coal devolatilization data*		(b) *Coal char combustion data*	
α_1 (s^{-1})	3.70×10^5	A (kg/(m^2 s $Pa^{0.5}$))	0.052
α_2 (s^{-1})	1.50×10^{13}	k (kJ/kmol)	6.10×10^4
k_1 (kJ $kmol^{-1}$)	7.40×10^4	Mechanism factor	2
k_2 (kJ $kmol^{-1}$)	2.50×10^5	Note: A and k may change for different coal types	

Typical parameters and wall boundary conditions employed in the simulation are listed in Tables 2–5.

The governing equations are discretized over a staggered grid using the finite difference method and integrated over each control volume in the computational domain. A non-uniform spacing of control volumes was used, placing more of them in regions near the burners and using a sufficient number of control volumes to obtain grid independent solutions. Each of the equations described in the above general form is tridiagonal and can be solved using TDMA solvers. The equations are solved by performing iterations until the solution satisfies a preset accuracy and SIMPLER algorithm [27] of pressure correction is applied in the iteration.

4. Model results

The computational domain simulates from the bottom up to the roof of the furnace. In this study, the computation domain was discretized using $17 \times 71 \times 90$ grid nodes while the radiative heat transfer equation was solved on a coarser grid with $14 \times 10 \times 34$ control volumes.

Figs. 3–5 show the temperature, oxygen and NO_x distribution in a vertical plane crossing the burners for Case 1 (100% boiler full load) and Case 4 (70% boiler full load), respectively. Comparison of the measured data (available for Cases 1, 4 and 5) with the calculated values are listed in Table 6. Tendency and agreement is found for all the cases except Case 5 (50% boiler full load). It is analysed that the models, especially the submodel of char combustion should be improved for an approved prediction of partial loads. The calculated results using the current models and

Table 5
Furnace wall boundary conditions

Wall	Side walls	Furnace bottom	Furnace exit	Furnace hopper	Platen superheaters
Emissivity	0.6	1	1	1	0.6
Wall temperature (K)	620	350	1000	350	620
Wall resistance	0	0	0	0	0

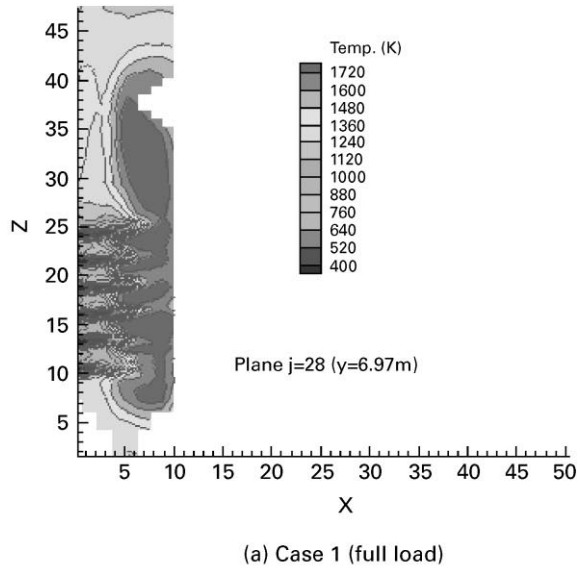

(a) Case 1 (full load)

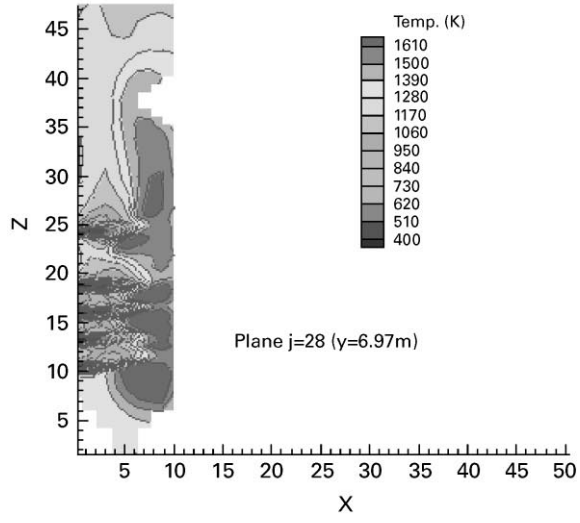

(b) Case 4 (70% full load)

Fig. 3. Temperature distribution of a section crossing burners.

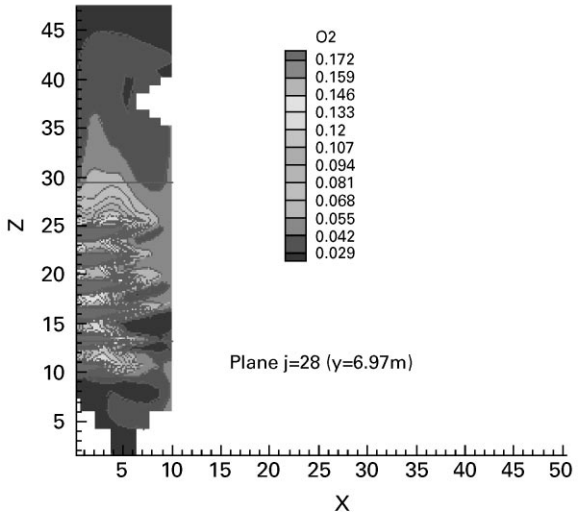

(a) Case 1 (full load)

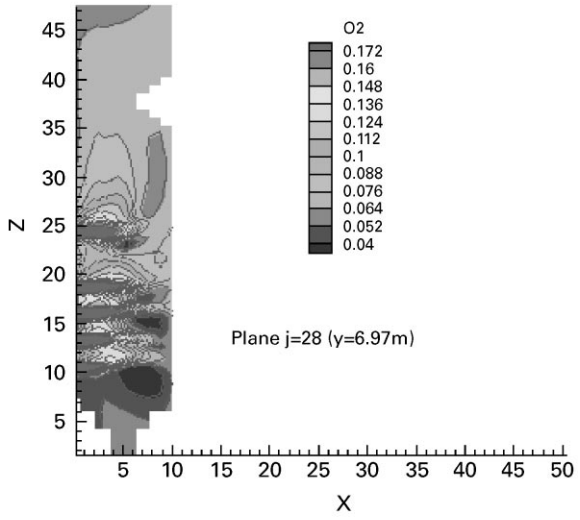

(b) Case 4 (70% full load)

Fig. 4. Oxygen distribution of a section crossing burners.

algorithm for higher loads are reasonable and can be applied.

A comparison of the calculated values for 100 and 70% boiler full load, without or with air leakage, is also listed in Table 6. It is shown that the furnace outlet temperature and total energy to walls are decreased with air leakage existing, while NO_x at the furnace outlet increased a little as expected. Better agreement between the measured values and the calculation results with air leakage than those without air leakage is found and this suggests that air leakage should be considered during boiler simulation. The calculated oxygen content is close to the experimental value. The calculated NO_x emission for full load decreases while from 50 to 70% load increases as observed. The results for full load presented some peculiarities where the predicted exit gas temperature is lower than the 95% case and the total heat to the boiler walls is smaller. This might be due to the fact of considering a linear scaling of the input parameters between the 70 and 100% load.

The increase of the air flow rate led as expected to a reduction of the furnace outlet temperature and to an increase in NO_x emissions. This shows that the NO_x model used in the current study can predict correctly NO_x changes with different oxygen levels in the furnace.

The maximum observed heat fluxes were compared with the predicted incident heat fluxes. The incident heat fluxes

Table 6
Measured data/calculated results for different cases

Case no.	1	4	5	6	9
Boiler load (%)	100	70	50	100	70
Furnace outlet temperature (K)	1530/1308	1290/1210	1208/1112	1530/1292	1290/1205
Furnace outlet O_2 (%)	2.29/1.65	3.22/2.32	4.40/4.94	2.29/2.80	3.22/3.18
Furnace outlet NO_x (ppm)	419.6/335.6	426.3/399.2	303.6/375.6	419.6/353.5	426.3/397.7
Total energy to walls (kW)	305000/346134	259000/312048	162000/242999	305000/341619	259000/306372

calculated based on clean wall conditions are in agreement with the maximum values observed. The maximum values are hard to define and the average wall conditions do not correspond to clean walls. Therefore based on the comparison of the measured values with the maximum heat fluxes a heat transfer resistance at the wall was estimated as about 10 m^2 K/KW. Considering this value uniformly at the walls leads to incident heat fluxes that are in general higher than the measured maximum values. The incident heat flux increases as expected when increasing the heat transfer resistance and therefore the gas temperature. The difference is probably due to the fact that the maximum values observed never correspond to a completely clean wall condition.

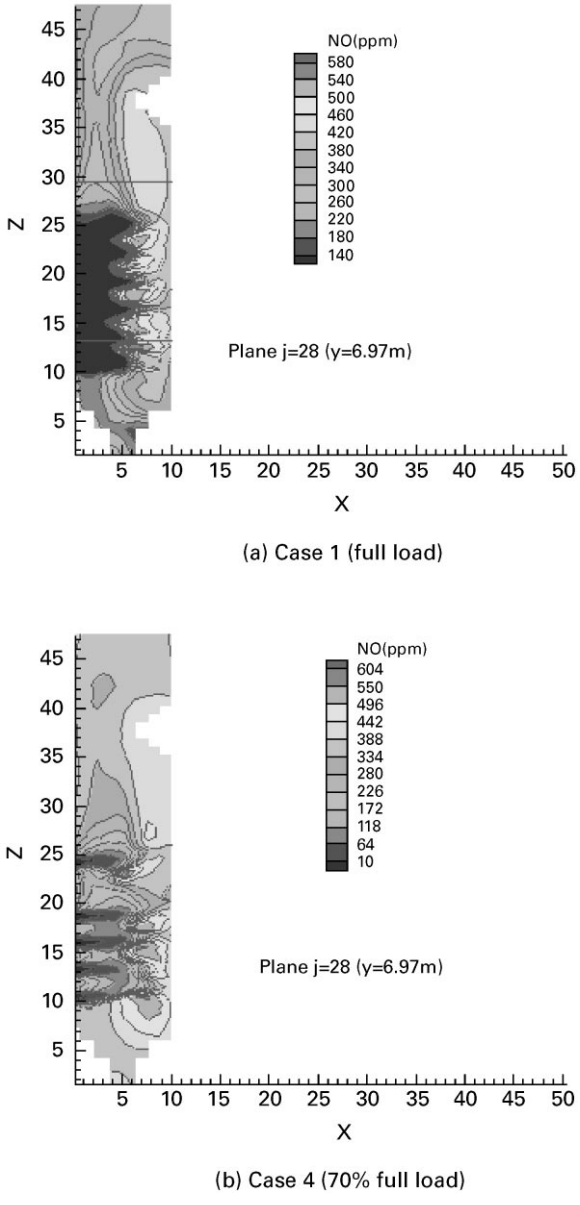

Fig. 5. NO_x distribution of a section crossing burners.

The comparison of the absorbed heat fluxes is presented in Fig. 6 showing an acceptable agreement with the heat flux readings. The correlation of the measurements with the calculations is close. The calculated values show smaller variation with position but the deviations due to the experimental data is well within the experimental uncertainty for these data.

The comparison of the heat flux data allow the conclusion that the information from the heat transfer calculations is representative of the reality and therefore the interest on the use of the model results to the support of heat transfer degradation calculations.

5. Conclusions

Three-dimensional simulation of the flow and combustion process in the furnace of a front wall pulverized coal-fired utility boiler was presented in this study. The tendency and agreement of the measured furnace outlet temperature, oxygen, NO_x, total heat energy transferred to walls and superheaters with calculated values was found for all the cases except the one of very low boiler load. Comparisons between measured data with calculated results, with and without air leakage to boiler furnace, suggest that the air leakage should be considered during boiler simulation.

Acknowledgements

This work was financed by the Commission of the European Community through subprogram ACORDE of the BRITE/EURAM Program under Contract No. BRPR-CT96-0198. The authors would like to express their gratitude to ENDESA for the contribution to the experimental data. Partial support from PRAXIS XXI/BPD/16323/98(No. 439.01) of FCT (Fundação para a Ciência e a Tecnologia) of the Ministry of Science and Technology of Portugal to Dr Minghou Xu is gratefully appreciated.

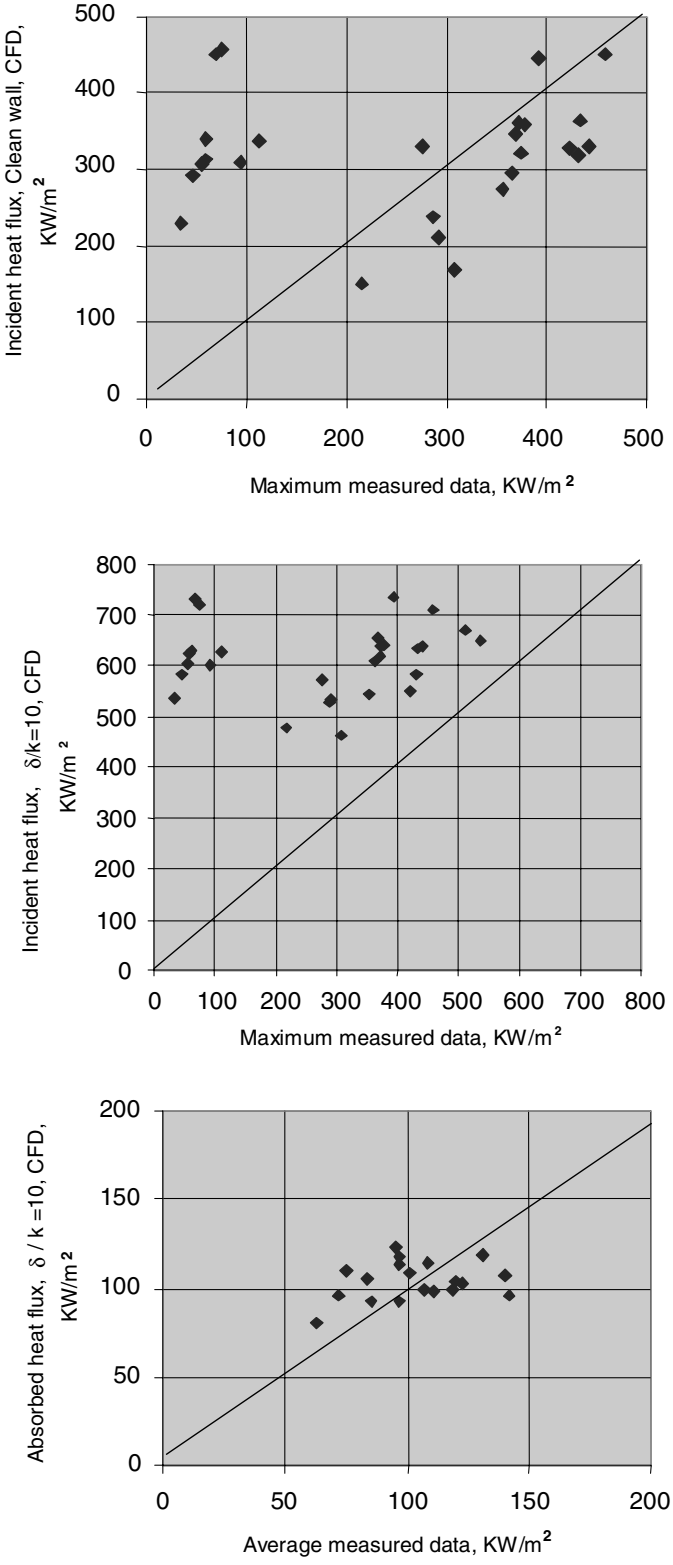

Fig. 6. Comparison of calculated heat flux with plant data.

References

[1] Boyd RK, Kent JH. Twenty-first Symposium (International) on Combustion. The Combustion Institute, Pittsburgh, 1986. p. 265–74.
[2] Robinson GF. J Inst Energy 1985:116–50.
[3] Görner K, Zinser W. ASME 107th Annual Meeting. Anaheim, California, USA, 1986.
[4] Lockwood FC, Papadopoulos C, Abbas AS. Combust Sci Technol 1988;58:5–24.
[5] Fiveland WA, Wessel RA. ASME J Engng Gas Turbines and Power 1988;110:117–26.
[6] Carvalho MG, Coelho P. Engng Comput 1991;7:227–324.
[7] Azevedo JLT, Coelho LMR, Carvalho MG. Combustion Related Organizations—Common and Unified Symposium. Salsomaggiore Terme, Italy, 1994. p. 11–7.
[8] Xu M, Yuan J, Ding S, Cao H. Comput Methods Appl Mech Engng 1998;155:369–80.
[9] Barlow SM. In: Durão et al, editors. Proceedings of International Symposium on Applied LDA to Fluid Mechanics. Lisbon, Portugal, 1982. p. 84.
[10] Costa M, Costen P, Lookwood FC. Combust Sci Technol 1991;75: 129–54.
[11] Wall TF, Stewart I, McC. J Inst Fuel 1975;May:235–40.
[12] Bonin MP, Queiroz M. Combust Flame 1991;85:121–33.
[13] Butler BW, Webb BW. Fuel 1991;70:1457–64.
[14] Lockwood FC, Shah NG. Eighteenth Symposium (International) on Combustion. The Combustion Institute, Pittsburgh, 1981. p. 1405–14.
[15] Azevedo JLT, Carvalho MG. Second Int Conf on Combustion Technologies for a Clean Environment. Lisbon, Portugal, 1993.
[16] Coimbra CFM, Azevedo JLT, Carvalho MG. Fuel 1994;73:1128–34.
[17] Yuan JW, Xu MH, Ding SF, Cao HD. Proc Third Int Symposium on Combustion. Beijing, China, 1995. p. 234–41.
[18] Xu MH, Yuan JW, Ding SF, Cao HD. Proc Chinese Soc Electl Engng 1996;16:266–70.
[19] Carvalho MG, Durão DFG, Pereira JCF. Engng Comput—Int J Computer Aided Engng Software 1987;4:23–34.
[20] Launder BE, Spalding DB. Comput Methods Appl Mech Engng 1974;3:269–89.
[21] Coelho PJ, Carvalho MG. Int J Numer Methods Engng 1993;36: 3401–19.
[22] De Soete GG. Fifteenth Symposium (International) on Combustion. The Combustion Institute, Pittsburgh, 1975. p. 1093–102.
[23] Chen W. A global reaction rate for nitric oxide reburning. PhD dissertation. Bringham Young University, 1994.
[24] Ubhayakar SK, Stickler DB, Rosenberg CWV, Gannon RE. Sixteenth Symposium (International) on Combustion. The Combustion Institute, Pittsburgh, 1977. p. 427–36.
[25] Kobayashi H, Howard JB, Sarofim AF. Sixteenth Symposium (International) on Combustion. The Combustion Institute, Pittsburgh, 1977. p. 411–24.
[26] Lockwood FC, Romo-Millares CA. J Institute Energy 1992;65:144–52.
[27] Patankar SV. Numerical heat transfer and fluid flow. New York: Hemisphere Publishing Corporation, 1980.